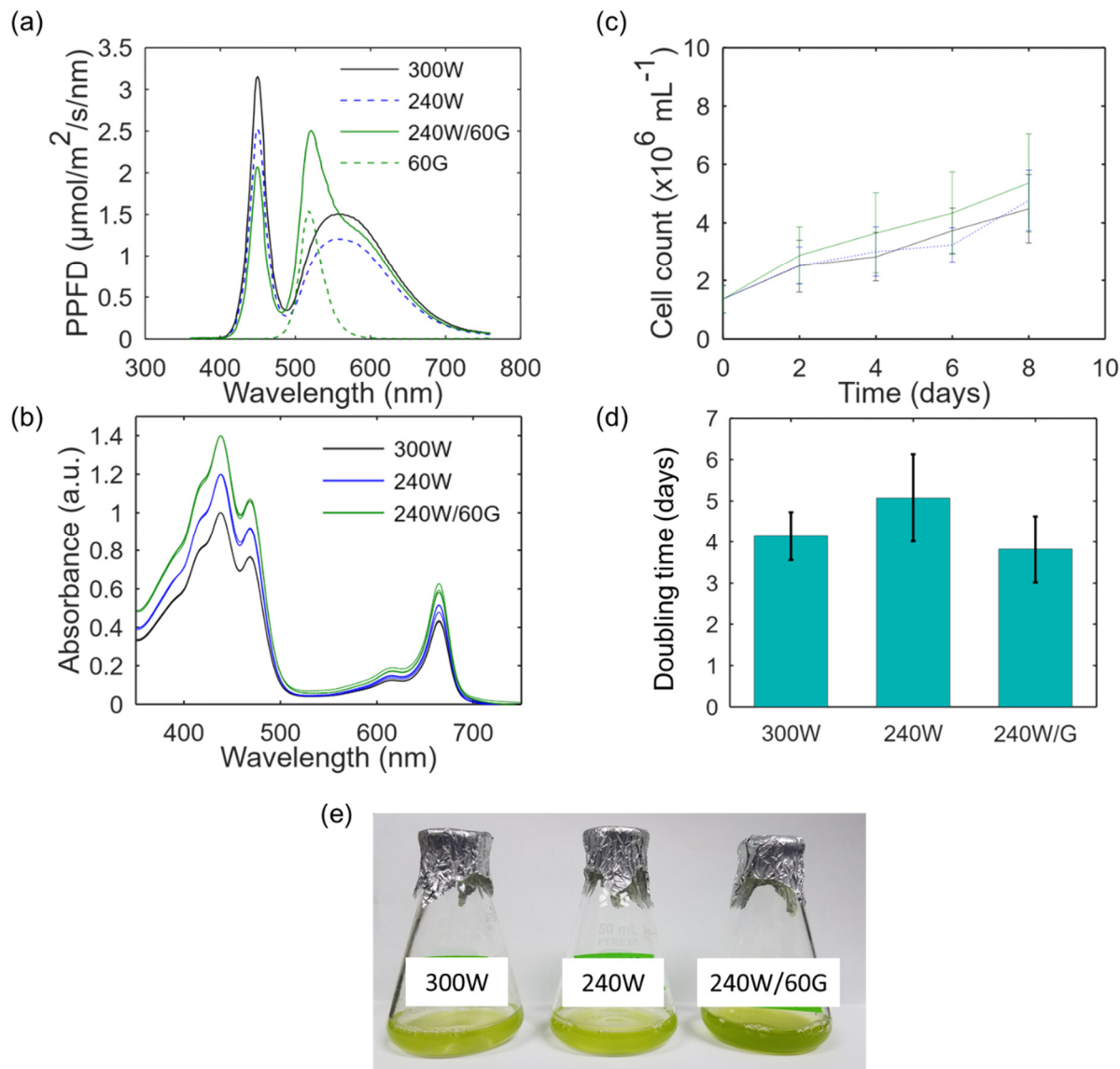
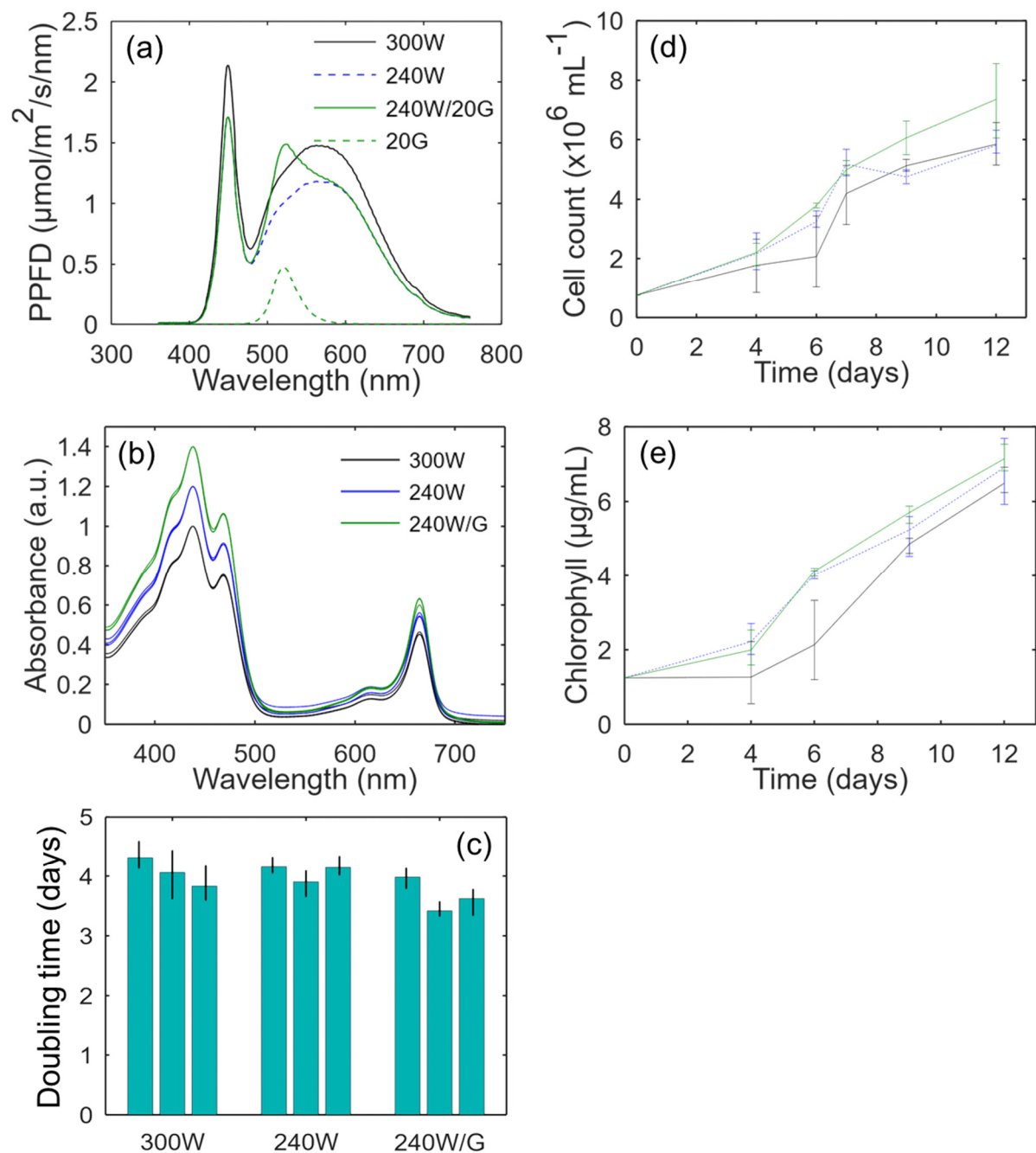


*Supplementary Information*

***A Phytophotonic Approach to Enhanced Photosynthesis***



**Figure S1.** (a) Spectral light profiles used in the first set of algae growth experiments (on spectral redistribution of light), measured using an LI-250A Light Meter (LI-COR®). (b) Chlorophyll profiles (extracted in methanol) of triplicate samples from each of the three lighting conditions, with samples within each set normalized to the same maximum value. (c) Cell count growth profiles over the full growth period, with error bars based on a nested ANOVA analysis of 6 biological replicates and 4 repeat measurements of each cell count. Note that the total sample volume was reduced after day 6 due to having extracted some sample for the chlorophyll measurements reported in the main text; after sampling the cultures continued to follow a normal, healthy growth curve despite this volume reduction. (d) Doubling time based on the cumulative growth period, with error bars based on a nested ANOVA analysis. (e) Photograph of three samples at the end of the growth period, one from each of the three lighting conditions.



**Figure S2.** (a) Spectral light profiles used in the second set of algae growth experiments (on temporal redistribution of light), measured using an LI-250A Light Meter (LI-COR®). (b) Chlorophyll profiles (extracted in methanol) of triplicate samples from each of the three lighting conditions, with each set normalized to the same maximum value. (c) Cell count and (d) chlorophyll growth profiles over the 12-day growth period, with error bars corresponding to minimum and maximum values.

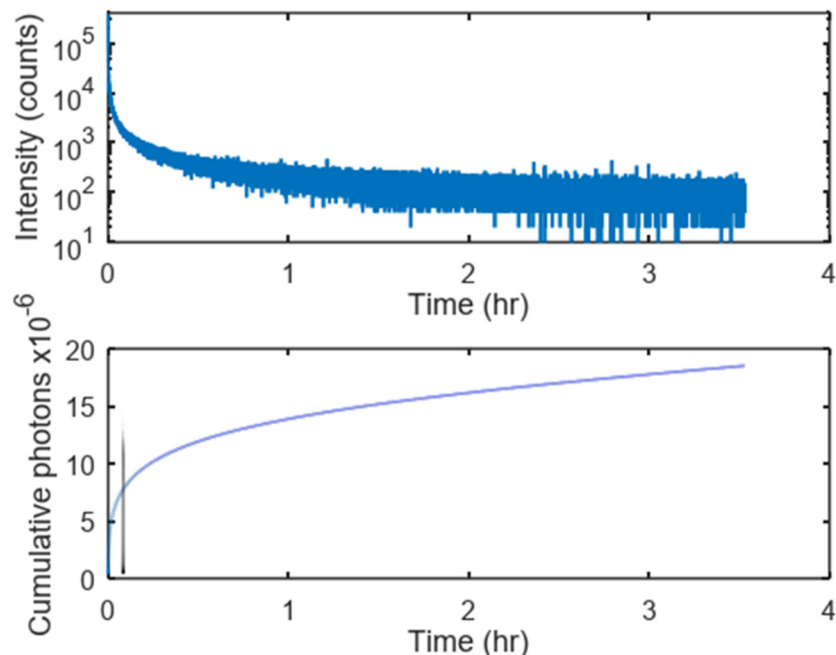


**Figure S3.** Long-term decay in luminescence intensity (top) and cumulative luminescence photon count (bottom) for a film of SrAl<sub>2</sub>O<sub>4</sub>:Eu,Dy in poly(methyl methacrylate). The intensity is seen to drop about 4 orders of magnitude over almost 4 hours, with about 40% of the luminescent photons being emitted within the first 5 minutes (see the vertical line). The sample, purchased from The Avid Colorist, has particles ranging from 50 – 75  $\mu\text{m}$  with a proprietary encapsulation, likely reducing recombination due to surface states. Of the commercial samples tested, this sample was second only to that from GloTech International in terms of PersL brightness and had the benefit of being more readily processible than the grains from GloTech, which are up to a few millimeters in size.

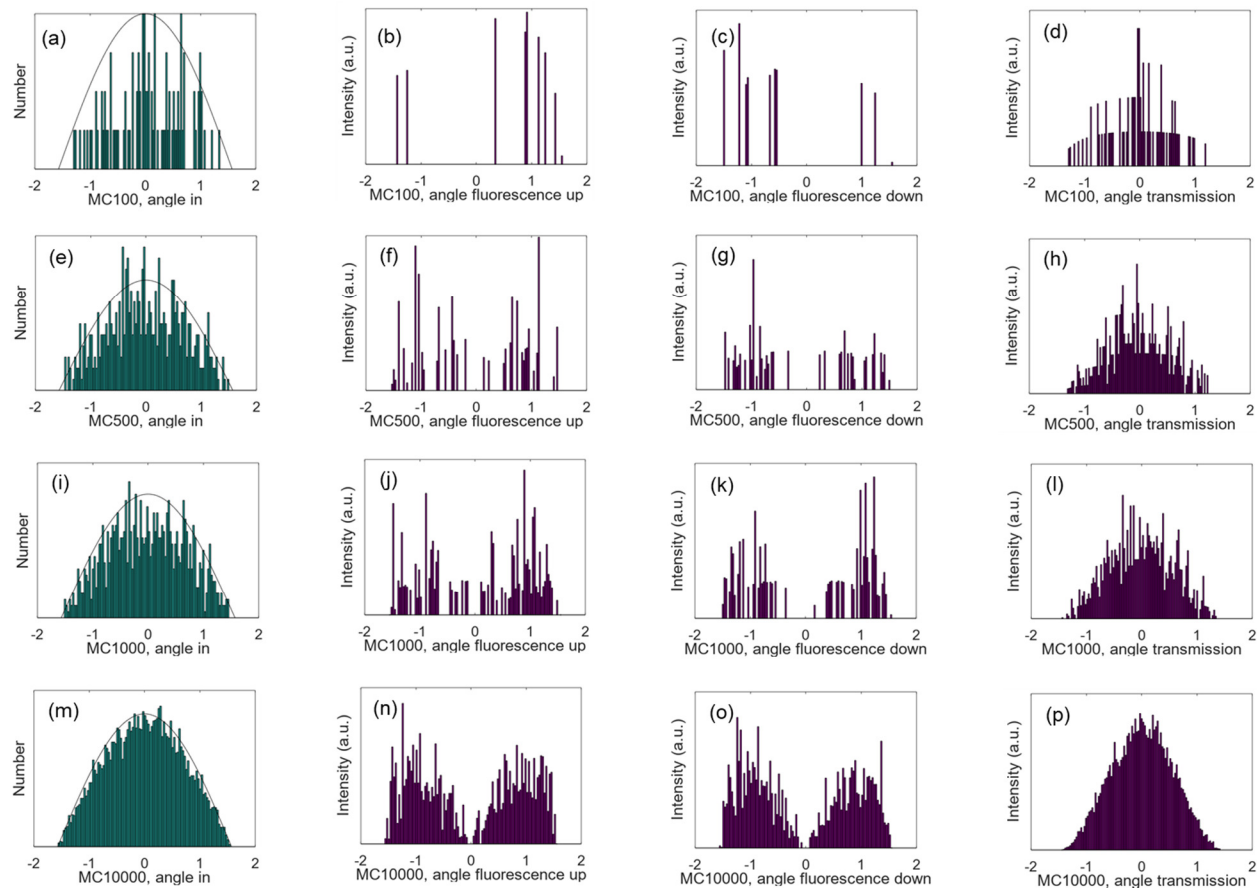


**Figure S4.** Convergence of the Monte Carlo (MC) simulation with increasing sample size from 100 (a-d) to 10,000 (m-p). The Monte Carlo angular distribution of the diffuse light entering the PersL concentrator (normalized by the number of samples) is shown in panels (a),(e),(i), and (m) alongside the analytical distribution (following Lambert's cosine law) from which these samples were drawn. The remaining panels show the intensity-weighted (after accounting for parasitic absorption) angular distribution of fluorescent light leaving the top of the concentrator, fluorescent light leaving the bottom of the concentrator, and light transmitted through the concentrator.

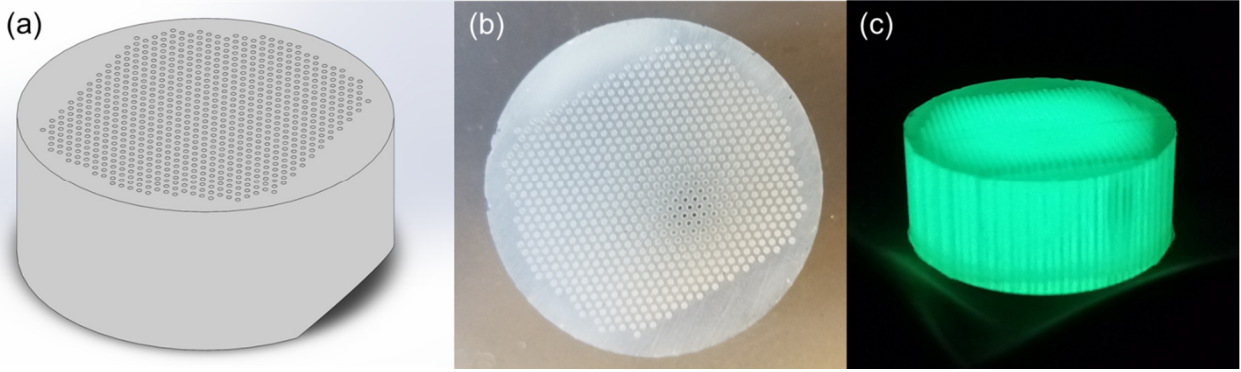


**Figure S5.** (a) CAD model of the PersL concentrator, “design 2,” with  $x = 800 \mu\text{m}$ ,  $w_{avg} = 1.3 \text{ mm}$ ,  $d = 400 \mu\text{m}$ , and  $h = 12.7 \text{ mm}$ . (b) Top view photograph of the PersL concentrator before filling the holes with  $\text{SrAl}_2\text{O}_4:\text{Eu,Dy}$  powder. (c) Photograph of the charged PersL concentrator,  $\sim 15 \text{ s}$  after transferring it from simulated sunlight to the dark.

## ***Experimental Methods for Algae Experiments***

Chlamydomonas strain: The *Chlamydomonas reinhardtii* strain used in this study was Wild-type CC-124 mt+ (137c). *Chlamydomonas reinhardtii* presents a useful model system for studying photosynthesis in higher plants.<sup>2</sup>

**Growth conditions for comparison of lighting profiles:** Cells were inoculated in purely phototrophic conditions in a HiPoint Plant growth chamber (FH-1200) at 23 °C under continuous, low-level white LED light (30  $\mu\text{mol photons m}^{-2} \text{s}^{-1}$ ), shaking at 130 rpm in 100 ml minimal medium (high-salt medium, HSM)<sup>3</sup> in 250 mL flasks to the mid-exponential growth phase (~10  $\mu\text{g/ml}$  chlorophyll). The white light spectrum used to cultivate the cells is shown in Figure S1. The medium was then refreshed by centrifugation (3000  $\times g$ , 2 min) and resuspension in minimal medium at a lower concentration of ~2  $\mu\text{g/ml}$  chlorophyll. The cells were grown in this refreshed medium under modified lighting for one day: diurnal (16 hrs light/day, including a 3-hr ramp on each end) high light (300  $\mu\text{mol/m}^2/\text{s}$ ), identical to the profile labelled as 300W in Figure 4. After this single day at high light, the culture was diluted slightly to set it to the initial cell and chlorophyll concentrations reported for each experiment (Figures 4, 5, S1, and S2), in the range of  $0.5 - 1 \times 10^6 \text{ ml}^{-1}$  and 1 – 2  $\mu\text{g/ml}$ , respectively. The algae were then split into separate samples in 15 ml HSM in 50 ml flasks. Six biological replicates were included for the spectral shift lighting conditions, and triplicate samples were included for the simulated shading lighting conditions. Experiments concerning spectral redistribution (Figures 4 and S1) were conducted in a HiPoint Plant growth chamber (FH-1200) and a Conviron Adaptis A1000-XT chamber at 23 °C, shaking samples at 130 rpm. Experiments concerning temporal redistribution (Figures 5 and S2) were conducted in a dark room under LED lighting, shaking samples at 180 rpm.

**Characterization of algae samples:** Cell counts and chlorophyll concentrations were monitored over the growth period. Each culture was sampled for a cell count measurement. To measure chlorophyll concentration, 1 ml of sample was removed from each sample, and pigments were extracted in methanol by centrifugation (15000  $\times g$ , 3 min), subsequent redissolution and vortex-mixing in methanol, and final centrifugation (15000  $\times g$ , 3 min) to isolate the pigments in the supernatant. Cell counts were measured using a Countess II Automated Cell Counter, and chlorophyll concentrations were measured using a Jenway Genova Plus Life Science Spectrophotometer after the extraction of the pigments in methanol. Significance of differences in cell count measurements was characterized with a mixed effects ANOVA p-value, where each measurement contains the contribution of a fixed light intensity effect and a random batch effect shared between replicates. Four repeat measurements were recorded for each cell count measurement of each biological replicate. Chl a/b ratios were calculated from UV/Vis absorption spectra of the extracted pigments (in methanol) collected with an Agilent Cary 6000i UV/Vis/NIR.  $F_v/F_m$  measurements were collected on dark-adapted samples with a DUAL-PAM-100 P700 & chlorophyll fluorescence measuring system. Samples were held in the dark for 20 minutes prior to the fluorescence measurements.

### ***Calculation of relative photosynthetic efficiency improvement needed***

Terrestrial biomass takes up about 120 GT-carbon/year, and anthropogenically generated CO<sub>2</sub> is accumulating in the atmosphere at a rate of 3-4 GT-carbon/year. For a conservative calculation, we assume 4 GT-carbon/year accumulation. In order to fix that additional atmospheric carbon as biomass without increasing the number of terrestrial plants, those plants would need to increase their carbon fixation efficiency by (4 GT-carbon/year)/(120 GT-carbon year), equivalent to a 3.3% *relative* increase in net photosynthetic efficiency. Here net photosynthetic efficiency means that this relative efficiency increase must account for respiration losses, which emit CO<sub>2</sub>.

### ***Details of the Photon Accounting Calculations for Lengthened Days***

AM1.0 solar insolation was used as the input spectrum, adjusted for angle of insolation over the course of the day. Calculations reported in the main text correspond to a latitude of 0.6532 radians 90 days past the spring equinox.

Absorption and emission kinetics were discretized in 1-s intervals, assuming 1 s of absorption and subsequent emission following a mono-exponential decay (of characteristic time  $\tau$ ) in intensity. The numbers of photons absorbed in 1 s ( $N_{abs,1s}$ ) and subsequently emitted over all time ( $N_{emit,tot}$ ) are conserved, accounting for a photoluminescent (PL) quantum yield below unity, such that  $N_{emit,tot} = (QY)N_{abs}$ . As a result, the emitted photons vary in time according to,

$$N_{emit}(t) = \frac{(QY)N_{abs}}{\tau} \exp\left(-\frac{t}{\tau}\right).$$

These absorption and emission behaviors were applied over time. A two-day simulation was run to account for overflow of emitted photons from the first day to the second for large values of  $\tau$ . Note there is a mismatch of time-scales inherent in this calculation: the condition  $\tau \gg t_{step}$  must be met to enable accurate integration of emitted photons over time, but simultaneously  $t_{step} \gtrsim 1s$  is needed over the two-day simulation due to limited memory (given the allotted computing resources); as such, this algorithm could only be applied over the range  $\tau \gtrsim 1000s$ .

These calculations were performed for three different sets of assumptions, all reported in the main text: (1) all photons at wavelengths below 500 nm are down-converted to PAR wavelengths with 100% efficiency; (2) 30% of PAR photons are down-converted to lower energy PAR wavelengths (e.g., converting blue/green to green/red wavelengths) with 50% efficiency; and (3) both UV and a fraction of PAR photons are down-converted to PAR wavelengths (Figure 8b). This efficiency encompasses both the quantum yield of PL and the capture efficiency of those PL photons. If the PersL material is embedded in a thin film, the downwards PL approaches 50% as the film thickness is decreased (approaching approximately a  $\mu\text{m}$ -scale, depending on the concentration and absorption cross-section of the PL material); meanwhile the upwards PL approaches 100% as the film thickness is increased (to the 100 $\mu\text{m}$ - to mm-scale, again depending on those same parameters). The capture efficiency of PL photons will thus depend on film thickness and how the film is used (i.e., above, within, or below the canopy). The mono-exponential decay assumed for these calculations is characteristic of a material with one dominant trap state. Materials like

SrAl<sub>2</sub>O<sub>4</sub>:Eu,Dy, with a multitude of different trap states at different energy levels, instead follow a poly-exponential decay.

### ***Details of the PersL Concentrator Monte Carlo Simulation***

Diffuse light travelling through the PersL concentrator was described as a collection of photon packets with a Monte Carlo simulation. The fraction of light incident on the pillars of SrAl<sub>2</sub>O<sub>4</sub>:Eu,Dy is immediately reflected or scattered back up. Photon packets incident normal to the top of the acrylic-component of the concentrator were assumed to scatter diffusely into the concentrator. The following algorithm was applied to each of these packets of incident photons:

- (1) The packet intersects a point on the top acrylic surface, with all points having an equal probability of occurrence.
- (2) The packet scatters diffusely downwards into the acrylic, at an angle pulled from a distribution following Lambert's cosine law.
- (3) The packet then travels, with some parasitic absorption by the acrylic, until intersecting a pillar of PersL material. Upon collision, it either scatters (with probability  $\sigma_{scat} = 0.99$ ) or is absorbed (with probability  $\sigma_{abs} = 0.01$ ).
  - a. Case 1 – scatter: the packet is elastically scattered further down the channel, assumed to have an angular dependence consistent with specular reflection. (In reality, surface roughness will lead to a combination of this specular reflection with diffuse scattering off the surface, further reducing overall transmission, consistent with the experimental measurements.) Parasitic absorption by the acrylic is calculated along the path to the subsequent collision.
  - b. Case 2 – absorption: if the photon packet is absorbed, it is re-emitted with reduced intensity (according to the quantum yield of photoluminescence, PL) at an angle characteristic of diffuse emission, pulled again from a distribution following Lambert's cosine law. Due to down-conversion implicit in the PL, this photon packet can no longer be absorbed by SrAl<sub>2</sub>O<sub>4</sub>:Eu,Dy. The parasitic absorption by the acrylic of the emitted photon packet is calculated along the packet's path out of the concentrator.

The simulation iterates over collisions until the photon packet either exits the bottom of the concentrator as a transmitted packet or is absorbed by the SrAl<sub>2</sub>O<sub>4</sub>:Eu,Dy.

- (4) The final fate of the photon packet is reported, indicating whether it exits the bottom or top of the concentrator as transmitted light or photoluminescence, and the final intensity and angle of travel.

Carrying out this algorithm in three dimensions is computationally intensive. Hence the path of each photon packet is instead described in two dimensions. The reasoning behind this reduction in dimensionality is shown schematically *via* the sample packet trajectory through the concentrator in Figure S6a. This path can be “unfolded” from a three-dimensional path to a two-dimensional path, collapsing the xy-plane into a single dimension for each photon packet. Along this unfolded

path, a mean distance between collisions (averaged over all possible angles, as shown in Figure S6) is used to describe the dimensionality-reduced spacing between pillars.

Based on known material properties of  $\text{SrAl}_2\text{O}_4:\text{Eu,Dy}$ , the quantum yield of PL was assumed to be 50% (an approximate, spectral average). The parasitic absorption by the acrylic was assumed to be  $0.01 \text{ mm}^{-1}$  along the path of travel, both appropriate for the material and yielding simulation results comparable to what was observed experimentally.

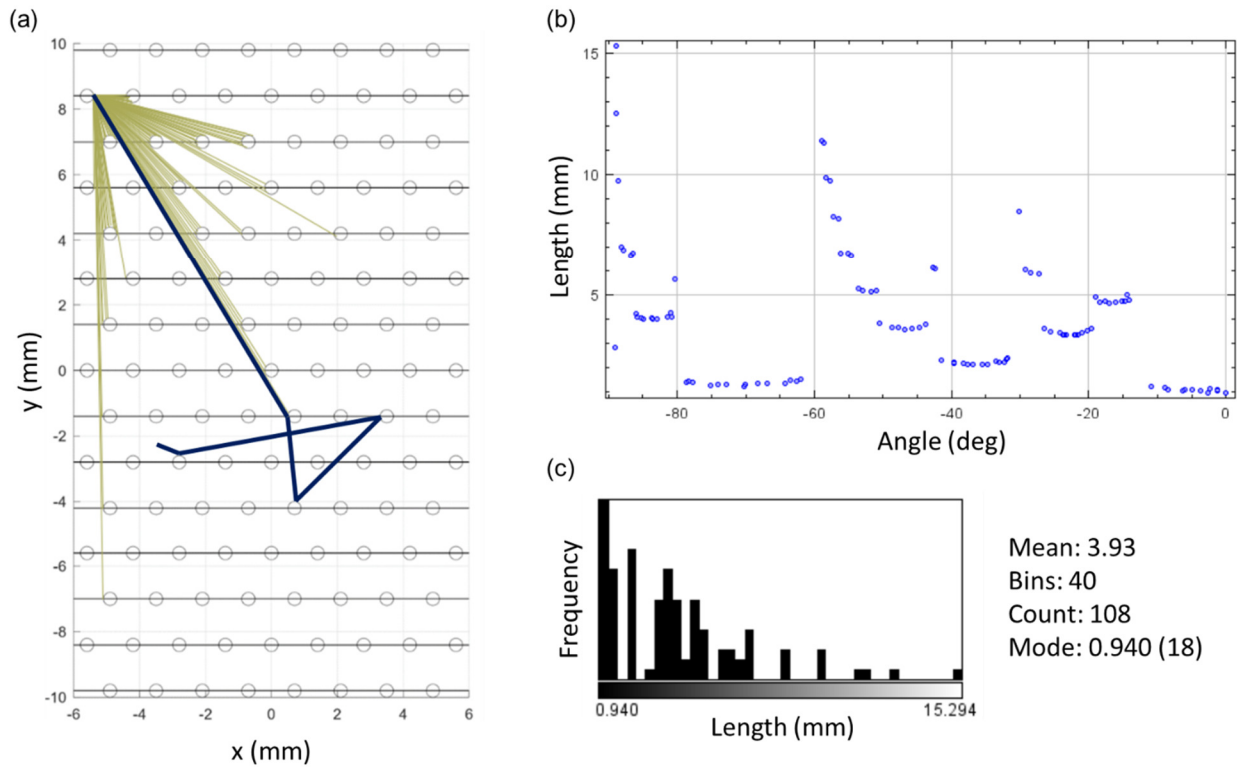


**Figure S6.** (a) A photon packet that collides with the right-most point of a  $\text{SrAl}_2\text{O}_4:\text{Eu,Dy}$  pillar can scatter / be re-emitted via PL at any angle from  $-\pi/2$  to  $\pi/2$  in the  $xy$ -plane; a stochastic spread of the possible trajectories is shown in green for half of this range, from  $-\pi/2$  to 0. The blue trajectory with five collisions in total describes one potential complete path through the concentrator (transmitted from top to bottom in this case). (b) The inter-collision path lengths are plotted for the stochastically sampled angles between  $-\pi/2$  and 0, shown in panel (a). These lengths are then binned in a histogram in panel (c).

## References

- <sup>1</sup> Ritchie, R.J. (2008) Universal chlorophyll equations for estimating chlorophylls a, b, c, and d and total chlorophylls in natural assemblages of photosynthetic organisms using acetone, methanol, or ethanol solvents. *Photosynthetica* 46, 115-126.
- <sup>2</sup> Harris, E.H. (2001) Chlamydomonas as a model organism. *Annu. Rev. Plant Physiol. Plant Mol. Biol.*, 52 (1), 363-406.
- <sup>3</sup> Sueoka, N. (1960) Mitotic Replication of Deoxyribonucleic Acid in Chlamydomonas Reinhardi. *PNAS* 46 (1), 83-91.